P122 | Advanced Topics in Plasma Physics

Double-Adiabatic Equations of State and Pressure Anisotropy

The Chew–Goldberger–Low (CGL) Equations

Instructor: Muni Zhou

How does a changing magnetic environment reshape a plasma's particle velocity distribution and pressure? When a plasma expands, compresses, or stretches, how do particle energies along and across the magnetic field change, and how does the resulting pressure affect the motion?

This question is relevant to many space and astrophysical plasmas. The expanding solar wind provides a concrete example: spacecraft measure unequal proton temperatures along and across the magnetic field. How does expansion generate this anisotropy, and why does the observed range narrow toward isotropy at higher plasma beta? These measurements motivate a description of pressure evolution and its consequences for plasma dynamics.

The CGL double-adiabatic laws provide a starting point: they predict how the perpendicular and parallel pressures change as density and magnetic-field strength evolve. We derive these laws heuristically from two particle adiabatic invariants; they can also be obtained from drift kinetics by taking moments and neglecting heat fluxes and collisions. We apply them to solar-wind expansion, then examine how collisions produce the Braginskii viscous response and how anisotropic stresses can drive firehose and mirror instabilities. The contrast between the CGL and kinetic mirror responses shows why pressure evolution sometimes requires a kinetic description.

Dartmouth College

Graduate plasma physics

Contents

1 Why pressure anisotropy matters in space **1**
1.1 Solar wind: two temperatures in an expanding plasma . . . 1
1.2 Pressure evolution and its consequences . . . 2
1.3 What the two pressures measure . . . 2
2 Two adiabatic invariants: a heuristic derivation of CGL **2**
2.1 First invariant: perpendicular temperature follows the field . . . 3
2.2 Second invariant: the parallel length determines parallel temperature . . . 3
2.3 The double-adiabatic equations of state . . . 4
3 How deformation produces pressure anisotropy **4**
3.1 Pressure changes and anisotropy production . . . 4
4 The collisional limit: Braginskii viscosity **5**
4.1 Add collisional isotropization . . . 5
4.2 Balance production against rapid collisions . . . 6
4.3 Write the result as a viscous stress . . . 6
4.4 Energy conversion and the scope of the result . . . 7
5 Pressure feedback and the parallel firehose **8**
5.1 Macroscopic equations and gyrotropic stress . . . 8
5.2 Pressure anisotropy changes magnetic tension . . . 9
5.3 Linearize a transverse perturbation . . . 9
6 Mirror instability and the Brazil plot **10**
6.1 Mirror response: a concrete test of the closure . . . 10
6.2 Return to the observations: the Brazil plot . . . 11
6.3 Outlook: why we need drift kinetics . . . 12
Recommended reading **13**
References **13**

1 Why pressure anisotropy matters in space

A spacecraft particle instrument measures a velocity distribution, not just a density and a temperature. When we resolve random velocities along and across the local magnetic field, their spreads need not be equal: $T_\parallel$ and $T_\perp$ can differ. For a given species, $p_\parallel = nk_BT_\parallel$ and $p_\perp = nk_BT_\perp$. This directional dependence is *pressure anisotropy*. It matters because the particles carry momentum and exchange energy differently in different directions.

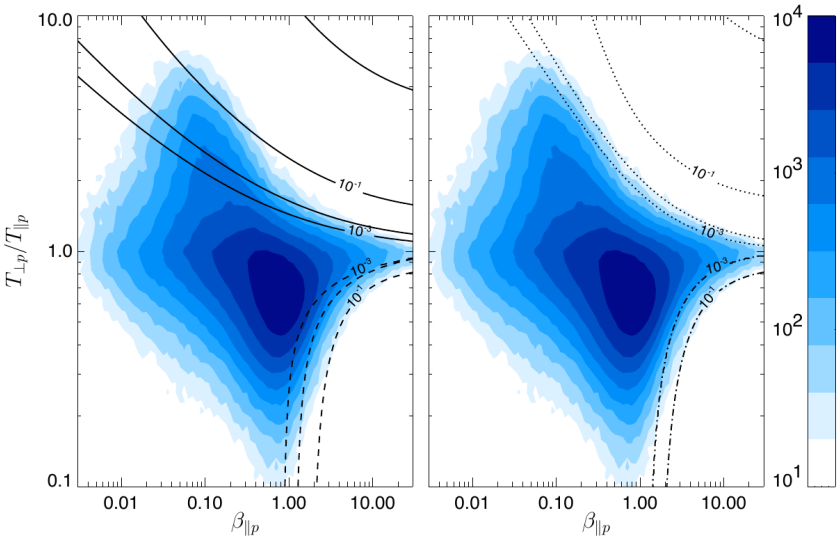
In a collisional gas, frequent collisions exchange energy among directions and make one temperature a useful approximation. A space plasma can instead remain strongly magnetized while collisions are too slow to maintain isotropy during expansion or compression. The field then provides a preferred direction, and the deformation of the plasma can change its velocity distribution. Solar-wind measurements show why we need to follow that change.

1.1 Solar wind: two temperatures in an expanding plasma

Start with the colored distribution in Figure 1. The axes locate each solar-wind sample by its proton temperature ratio and parallel beta:

$$R_p = \frac{T_{\perp p}}{T_{\parallel p}}, \qquad \beta_{\parallel p} = \frac{8\pi n_p k_B T_{\parallel p}}{B^2}. \tag{1.1}$$

Here beta compares parallel particle pressure with magnetic pressure, in Gaussian-cgs units. The horizontal level $R_p = 1$ represents equal temperatures. Samples above and below it have opposite signs of pressure anisotropy. The color indicates how frequently different states occur; it is not wave power.



What to notice. The measurements occupy a broad range on both sides of isotropy. At higher beta, most lie between the mirror and oblique-firehose growth-rate contours in the right-hand panel, and the occupied range narrows toward $R_p = 1$. These are statistical constraints, rather than perfectly sharp walls around every measurement.

Figure 1: Wind/SWE proton measurements from 1995–2001 for $v_{\rm sw} \leq 600\,{\rm km\,s^{-1}}$. Both panels contain the same observed distribution. The overlaid curves are kinetic growth-rate contours: proton cyclotron and parallel firehose on the left, mirror and oblique firehose on the right.

The question for CGL. What drives the plasma away from equal temperatures, and what limits the resulting anisotropy? As a parcel of solar-wind plasma travels outward from the Sun, its density decreases and its magnetic field changes. CGL predicts how these changes drive the two temperatures apart (the solar-wind example in Section 3). Instability and subsequent regulation address the limits of that evolution (Section 6.2). We need both parts to interpret the observed distribution.

1.2 Pressure evolution and its consequences

The solar-wind observation leads to three connected questions. First, how does a changing field and density redistribute random particle energy between directions? Second, how do the resulting pressures affect the flow and magnetic field? Third, when do heat transport, collisions, or growing waves change that response? We can answer the first two before developing a theory of kinetic instabilities.

There is also a useful quantitative reason to care about apparently small anisotropy. For one species, or for consistently defined total pressures, let $R = p_\perp/p_\parallel$ and $\beta_\parallel = 8\pi p_\parallel/B^2$. Then

$$\frac{p_\perp - p_\parallel}{B^2/(8\pi)} = \beta_\parallel(R-1). \tag{1.2}$$

At $\beta_\parallel = 100$, a one-percent pressure difference is already comparable in magnitude to the magnetic pressure. This comparison does not by itself establish instability. It tells us why a distribution that looks nearly isotropic can still have an important effect on magnetic forces.

The purpose of CGL in this lecture. Given a smooth deformation of a magnetized plasma element, predict $p_\perp$ and $p_\parallel$, then use their stress to calculate the subsequent motion. This gives us directional heating and cooling and the pressure contribution to the tension of a bent field line. These are useful predictions even when no instability develops. Later, comparing this adiabatic response with observations tells us which additional physics a pressure model may need.

Conventions. We use Gaussian-cgs units, $D/Dt = \partial_t + \boldsymbol{u}\cdot\boldsymbol{\nabla}$, and $\Delta p = p_\perp - p_\parallel$. Temperatures are in kelvin. Magnetic pressure is $B^2/(8\pi)$; in SI it is $B^2/(2\mu_0)$.

1.3 What the two pressures measure

Separate bulk motion from random motion: $\boldsymbol{w} = \boldsymbol{v} - \boldsymbol{u}$. Choose the local z direction along $\boldsymbol{B}$. On scales slow compared with gyromotion, average over the gyrophase; the two perpendicular directions are then equivalent. This is *gyrotropy*. The pressure tensor in these local coordinates is

$$\mathsf{P} = \begin{pmatrix} p_\perp & 0 & 0 \\ 0 & p_\perp & 0 \\ 0 & 0 & p_\parallel \end{pmatrix} = p_\perp(\mathsf{I} - \boldsymbol{bb}) + p_\parallel \boldsymbol{bb}, \qquad \boldsymbol{b} = \frac{\boldsymbol{B}}{B}. \tag{1.3}$$

Pressure measures random momentum flux in a direction. Thus

$$p_\perp = \frac{mn}{2}\left\langle w_x^2 + w_y^2 \right\rangle = nk_B T_\perp, \qquad p_\parallel = mn\left\langle w_z^2 \right\rangle = nk_B T_\parallel. \tag{1.4}$$

For $n = \int f\,\mathrm{d}^3w$, the brackets mean $\langle G\rangle = n^{-1}\int Gf\,\mathrm{d}^3w$. Gyrotropy makes the two perpendicular directions equivalent; it does not require $p_\perp = p_\parallel$ or a Maxwellian distribution. The random energy density is

$$\boxed{U = p_\perp + \frac{1}{2}p_\parallel.} \tag{1.5}$$

Two perpendicular degrees of freedom contribute $p_\perp$; the one parallel degree contributes $p_\parallel/2$. This counting will determine the parallel temperature response.

2 Two adiabatic invariants: a heuristic derivation of CGL

The perpendicular and parallel random motions have different adiabatic responses. Averaging those responses gives two pressure laws.

Assume strong magnetization, $\omega_{\rm dyn} \ll \Omega_s$ and $\rho_s \ll L$, and neglect collisions and heat transport during the evolution. The first condition permits gyroaveraging and magnetic-moment conservation; it does not, by itself, eliminate parallel heat transport. The second-invariant argument below is a heuristic way to obtain the parallel law.

2.1 First invariant: perpendicular temperature follows the field

For slowly varying fields, the first particle adiabatic invariant is

$$\mu = \frac{m w_\perp^2}{2B} \simeq \text{const.} \tag{2.1}$$

Its average over a locally uniform distribution is

$$\langle \mu \rangle = \frac{1}{n} \int \frac{m w_\perp^2}{2B} f \, \mathrm{d}^3 w = \frac{p_\perp}{nB} = \frac{k_B T_\perp}{B}. \tag{2.2}$$

With negligible heat transport and scattering, this average is carried with the fluid element. Therefore

$$\boxed{\frac{D}{Dt}\left(\frac{p_\perp}{nB}\right) = 0, \qquad T_\perp \propto B.} \tag{2.3}$$

A stronger field raises the perpendicular random energy per particle, $p_\perp/n = k_B T_\perp$. This is the magnetic-moment argument behind betatron energization. The changing electromagnetic configuration supplies the energy through electric fields; the magnetic force itself does no work on a particle.

2.2 Second invariant: the parallel length determines parallel temperature

For a particle bouncing periodically between magnetic mirrors, the second adiabatic invariant is the longitudinal action,

$$J = \oint m w_\parallel \, \mathrm{d}s. \tag{2.4}$$

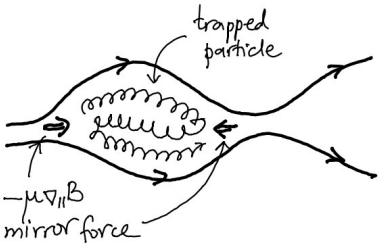


Figure 2: Particles bounce between the strong-field ends of a magnetic bottle; their bounce action is J. Magnetic trapping alone does not imply the collective mirror instability (Section 6.1).

It is approximately conserved when the configuration changes slowly compared with a bounce period. For the simple slowly deforming trap used in this heuristic picture, J scales as $m w_\parallel \ell$, where ℓ is the parallel extent. Thus $\langle J^2 \rangle \propto m^2 \ell^2 \left\langle w_\parallel^2 \right\rangle$ is conserved.

How does ℓ change? Take a thin tube with cross section $\mathcal{A}$, volume $\mathcal{A}\ell$, and fixed particle content and magnetic flux:

$$n\mathcal{A}\ell = \text{const}, \qquad B\mathcal{A} = \text{const}. \tag{2.5}$$

Dividing the first relation by the second gives

$$\frac{n\ell}{B} = \text{const} \quad \Longrightarrow \quad \boxed{\ell \propto \frac{B}{n}.} \tag{2.6}$$

Use $p_\parallel = mn \left\langle w_\parallel^2 \right\rangle$ to convert the particle scaling into a pressure law:

$$\left\langle J^2 \right\rangle \propto m \frac{p_\parallel}{n} \ell^2 \propto m \frac{p_\parallel B^2}{n^3} \simeq \text{const}. \tag{2.7}$$

Hence

$$\boxed{\frac{D}{Dt}\left(\frac{p_\parallel B^2}{n^3}\right) = 0, \qquad T_\parallel \propto \frac{n^2}{B^2}.} \tag{2.8}$$

Shortening the parallel extent increases the parallel random speed and temperature; lengthening it has the opposite effect.

2.3 The double-adiabatic equations of state

Combining the two results gives the Chew–Goldberger–Low laws:

$$\boxed{\frac{D}{Dt}\left(\frac{p_\perp}{nB}\right) = 0, \qquad \frac{D}{Dt}\left(\frac{p_\parallel B^2}{n^3}\right) = 0.} \tag{2.9}$$

The constants follow the plasma element. Density and field strength therefore determine two different temperatures, rather than a single isotropic equation of state.

The name *double-adiabatic equations of state* reflects the two adiabatic pressure laws, which this heuristic derivation associates with conservation of μ and J.

A solar-wind parcel need not be a magnetic bottle: the literal bounce action applies to periodic particle orbits. Using a parallel element length is a heuristic extension of that picture. The fluid laws can also follow from a gyrotropic kinetic description without requiring every particle to be trapped. Their essential extra assumption is negligible heat transport, which particle adiabatic invariance alone does not ensure. We will return to this limitation when comparing CGL with the mirror response.

3 How deformation produces pressure anisotropy

The flux-tube picture gives the pressure response to finite changes in density and magnetic-field strength. To find how quickly anisotropy develops, we now follow these changes along a moving plasma element.

3.1 Pressure changes and anisotropy production

Take logarithmic derivatives of the two CGL laws, $p_\perp/(nB) = \text{const}$ and $p_\parallel B^2/n^3 = \text{const}$:

$$\boxed{\begin{aligned} \frac{Dp_\perp}{Dt} &= p_\perp\left(\frac{D\ln n}{Dt} + \frac{D\ln B}{Dt}\right), \\ \frac{Dp_\parallel}{Dt} &= p_\parallel\left(3\frac{D\ln n}{Dt} - 2\frac{D\ln B}{Dt}\right). \end{aligned}} \tag{3.1}$$

Here D/Dt follows the element. Density changes affect both pressures, while field amplification increases the perpendicular pressure and decreases the parallel pressure at fixed density. Subtracting their logarithmic derivatives gives the evolution of $R = p_\perp/p_\parallel$:

$$\boxed{\frac{D\ln R}{Dt} = 3\frac{D\ln B}{Dt} - 2\frac{D\ln n}{Dt} = 3\frac{D}{Dt}\ln\left(\frac{B}{n^{2/3}}\right).} \tag{3.2}$$

Thus the ratio grows when $B/n^{2/3}$ increases and falls when it decreases. Isotropic compression has $B \propto n^{2/3}$, so it preserves R and generates no anisotropy from an initially isotropic plasma.

For the collisional calculation later, we also need the pressure difference $\Delta p = p_\perp - p_\parallel$. Define the mean pressure by

$$p = \frac{2p_\perp + p_\parallel}{3}, \qquad p_\perp = p + \frac{\Delta p}{3}, \quad p_\parallel = p - \frac{2\Delta p}{3}. \tag{3.3}$$

Near isotropy, set $p_\perp \simeq p_\parallel \simeq p$ on the right-hand sides of (3.1) and subtract:

$$\boxed{\frac{D\Delta p}{Dt} \simeq 3p\left(\frac{D\ln B}{Dt} - \frac{2}{3}\frac{D\ln n}{Dt}\right).} \tag{3.4}$$

This is the leading production of pressure anisotropy by a changing field and density. In Section 4, collisions will compete with this production by relaxing the pressure difference.

Example: solar-wind expansion. Follow an initially isotropic parcel of solar-wind plasma as it moves outward from the Sun. Consider only its slow expansion, neglecting heat transport, collisions, and feedback from waves. For a steady, constant-speed radial flow with a radial magnetic field, particle and magnetic flux conservation give $n \propto r^{-2}$ and $B \propto r^{-2}$. The CGL laws then give

$$T_\perp \propto B \propto r^{-2}, \qquad T_\parallel \propto \frac{n^2}{B^2} = \text{const.} \tag{3.5}$$

The perpendicular temperature falls while the parallel temperature stays constant: expansion alone therefore produces $p_\parallel > p_\perp$.

The same expansion also changes beta. With $R = T_\perp/T_\parallel$ and $\beta_\parallel = 8\pi n k_B T_\parallel/B^2$, the parcel follows

$$\boxed{R \propto r^{-2}, \qquad \beta_\parallel \propto r^2, \qquad R\beta_\parallel = \text{const.}} \tag{3.6}$$

On a Brazil plot, the parcel starts at $R = 1$ and moves down and to the right: smaller R and larger $\beta_\parallel$. These are two consequences of the same expansion; increasing beta is not an independent cause of the anisotropy.

This is the trajectory driven by expansion alone. In a real plasma, other physical effects can oppose the increasing anisotropy and change that trajectory. We will consider two:

1. **Collisions between particles** redistribute random energy between directions and relax $p_\perp - p_\parallel$ toward zero.
2. **Fluid and kinetic instabilities** can grow once the anisotropy is sufficiently strong relative to magnetic stresses; the resulting fluctuations can modify the pressure evolution.

We begin with collisions: balancing collisional relaxation against anisotropy production gives the Braginskii viscous response. We then turn to the collective instabilities, starting with firehose and mirror.

4 The collisional limit: Braginskii viscosity

We first let collisions oppose the adiabatic production of anisotropy. If collisional relaxation is rapid compared with the changing flow, its balance with production gives the leading parallel viscous stress.

4.1 Add collisional isotropization

Recall $p = (2p_\perp + p_\parallel)/3$. Add collisional relaxation toward this mean pressure:

$$\frac{Dp_\perp}{Dt} = p_\perp\left(\frac{D\ln n}{Dt} + \frac{D\ln B}{Dt}\right) - \nu(p_\perp - p), \tag{4.1}$$

$$\frac{Dp_\parallel}{Dt} = p_\parallel\left(3\frac{D\ln n}{Dt} - 2\frac{D\ln B}{Dt}\right) - \nu(p_\parallel - p). \tag{4.2}$$

Since $p_\perp - p = \Delta p/3$ and $p_\parallel - p = -2\Delta p/3$, these terms conserve the random energy $U = p_\perp + p_\parallel/2$ and relax Δp at rate ν. Subtract the two equations:

$$\frac{D\Delta p}{Dt} + \nu\Delta p = (p_\perp + 2p_\parallel)\frac{D\ln B}{Dt} + (p_\perp - 3p_\parallel)\frac{D\ln n}{Dt}. \tag{4.3}$$

For $|\Delta p| \ll p$, replace $p_\perp$ and $p_\parallel$ by p on the right:

$$\boxed{\frac{D\Delta p}{Dt} + \nu\Delta p \simeq 3p\frac{D}{Dt}\ln\left(\frac{B}{n^{2/3}}\right).} \tag{4.4}$$

The right side is the CGL production rate; the collision term removes anisotropy. This is a model collision term: it captures isotropization and energy conservation, rather than the full Coulomb collision operator.

4.2 Balance production against rapid collisions

Use the strongly magnetized, collisional ordering

$$\omega_{\rm dyn},\ |\boldsymbol{\nabla u}| \ll \nu_{ii} \ll \Omega_i, \qquad k_\parallel \lambda_{\rm mfp} \ll 1, \qquad \lambda_{\rm mfp} \sim v_{{\rm th},i}/\nu_{ii}. \tag{4.5}$$

Here $\nu \sim \nu_{ii}$ for the ion stress. Gyromotion is fastest, but collisions are fast compared with the changing flow. After the initial relaxation, $D\Delta p/Dt \sim \omega_{\rm dyn}\Delta p$ is smaller than $\nu\Delta p$. Dropping it in (4.4) gives

$$\boxed{\Delta p \simeq \frac{3p}{\nu}\frac{D}{Dt}\ln\left(\frac{B}{n^{2/3}}\right) = 3\eta_\parallel\left(\frac{D\ln B}{Dt} - \frac{2}{3}\frac{D\ln n}{Dt}\right), \qquad \eta_\parallel = \frac{p}{\nu}.} \tag{4.6}$$

This balance also gives $|\Delta p|/p \sim \omega_{\rm dyn}/\nu \ll 1$, consistent with the expansion. The stress is determined by the current deformation rate. Coulomb kinetics supplies the numerical coefficient in $\eta_\parallel \sim p_i/\nu_{ii}$; the relaxation model obtains its form and scaling.

4.3 Write the result as a viscous stress

This subsection explains *why the pressure anisotropy obtained above acts as a viscous stress.* The next subsection explains how that stress converts macroscopic flow energy into the energy of random particle motion. We first take the magnetic field along z and use ordinary velocity derivatives.

From changes in B and n to velocity gradients. For a small material element, $\partial u_x/\partial x$, $\partial u_y/\partial y$, and $\partial u_z/\partial z$ are the fractional stretching rates in the three directions. Their sum, $\boldsymbol{\nabla}\cdot\boldsymbol{u}$, is the fractional volume-change rate. Conservation of particles therefore gives $D\ln n/Dt = -\boldsymbol{\nabla}\cdot\boldsymbol{u}$.

With a locally straight field along z, the area perpendicular to the field changes at rate $\partial u_x/\partial x + \partial u_y/\partial y$. Frozen magnetic flux through that material area gives

$$\frac{D\ln B}{Dt} = -\left(\frac{\partial u_x}{\partial x} + \frac{\partial u_y}{\partial y}\right) = \frac{\partial u_z}{\partial z} - \boldsymbol{\nabla}\cdot\boldsymbol{u}.$$

Substitute these density and field-strength changes into the collisional balance (4.6):

$$\boxed{\Delta p = 3\eta_\parallel\left(\frac{\partial u_z}{\partial z} - \frac{1}{3}\boldsymbol{\nabla}\cdot\boldsymbol{u}\right).} \tag{4.7}$$

The parentheses measure the *stretching rate along the field minus the average stretching rate in the three directions.* Isotropic compression has equal rates in all three directions, so this difference vanishes: it produces no new anisotropy. Ordinary adiabatic compression can still raise the temperature.

How the pressure difference becomes a viscous force. Recall $p_\perp = p + \Delta p/3$ and $p_\parallel = p - 2\Delta p/3$. In these coordinates,

$$\mathsf{P} = \begin{pmatrix} p_\perp & 0 & 0 \\ 0 & p_\perp & 0 \\ 0 & 0 & p_\parallel \end{pmatrix} = p\mathsf{I} + \boldsymbol{\Pi}, \qquad \boldsymbol{\Pi} = \begin{pmatrix} \Delta p/3 & 0 & 0 \\ 0 & \Delta p/3 & 0 \\ 0 & 0 & -2\Delta p/3 \end{pmatrix}. \tag{4.8}$$

Thus $\boldsymbol{\Pi}$ is simply the part of the pressure that differs from its directional average. The pressure force splits into $-\boldsymbol{\nabla}p - \boldsymbol{\nabla}\cdot\boldsymbol{\Pi}$. In the collisional balance, Δp and hence $\boldsymbol{\Pi}$ are proportional to velocity gradients; taking the divergence supplies a second derivative.

For a concrete example, let $\boldsymbol{u} = u_z(z)\,\hat{\boldsymbol{z}}$. Now $\boldsymbol{\nabla}\cdot\boldsymbol{u} = \partial u_z/\partial z$, so

$$\Delta p = 2\eta_\parallel \frac{\partial u_z}{\partial z}, \qquad \Pi_{zz} = -\frac{2}{3}\Delta p = -\frac{4}{3}\eta_\parallel \frac{\partial u_z}{\partial z}.$$

If $\eta_\parallel$ is approximately uniform, the extra force per unit volume is

$$-\frac{\partial \Pi_{zz}}{\partial z} = \frac{4}{3}\eta_\parallel \frac{\partial^2 u_z}{\partial z^2}. \tag{4.9}$$

This has the familiar form of a viscous force: it smooths velocity variations. For example, a sinusoidal velocity perturbation has $\partial_z^2 u_z = -k^2 u_z$, so the force opposes that perturbation. The essential step is the collisional relation between stress and the *current* velocity gradient; pressure anisotropy alone need not be dissipative.

General field direction. For $\boldsymbol{b} = \boldsymbol{B}/B$, the shorthand $\boldsymbol{bb} : \boldsymbol{\nabla u}$ means the stretching rate along the local field: $\sum_{i,j} b_i b_j\, \partial u_j/\partial x_i$. It reduces to $\partial u_z/\partial z$ in our example. Continuity and ideal induction give

$$\frac{D\ln n}{Dt} = -\boldsymbol{\nabla}\cdot\boldsymbol{u}, \qquad \frac{D\ln B}{Dt} = \boldsymbol{bb} : \boldsymbol{\nabla u} - \boldsymbol{\nabla}\cdot\boldsymbol{u}, \tag{4.10}$$

so the same difference of stretching rates is

$$\frac{D\ln B}{Dt} - \frac{2}{3}\frac{D\ln n}{Dt} = \boldsymbol{bb} : \boldsymbol{\nabla u} - \frac{1}{3}\boldsymbol{\nabla}\cdot\boldsymbol{u}. \tag{4.11}$$

The component result above can then be written compactly as

$$\boxed{\begin{aligned} \Delta p &= 3\eta_\parallel \left(\boldsymbol{bb} : \boldsymbol{\nabla u} - \frac{1}{3}\boldsymbol{\nabla}\cdot\boldsymbol{u}\right), \\ \boldsymbol{\Pi} &= -\Delta p \left(\boldsymbol{bb} - \frac{\mathsf{I}}{3}\right). \end{aligned}} \tag{4.12}$$

These are the same pressure difference and stress expressed for an arbitrary field direction. Here $\boldsymbol{\Pi}$ is the anisotropic part of the *pressure* tensor, so its force enters with a minus sign, $-\boldsymbol{\nabla}\cdot\boldsymbol{\Pi}$.

4.4 Energy conversion and the scope of the result

This subsection explains *how the viscous stress converts macroscopic flow energy into random particle energy.* As viscosity damps a flow, the lost flow energy appears as heat. We can see the transfer by calculating the work done by the pressures in each direction.

Pressure work with the field along z. For an isotropic gas, the pressure work per unit volume per unit time is $-p\boldsymbol{\nabla}\cdot\boldsymbol{u}$: compression makes this positive. With two different pressures, add the work in each direction instead:

$$\begin{aligned} &-p_\perp \frac{\partial u_x}{\partial x} - p_\perp \frac{\partial u_y}{\partial y} - p_\parallel \frac{\partial u_z}{\partial z} \\ &\qquad = -p\boldsymbol{\nabla}\cdot\boldsymbol{u} + \Delta p \left(\frac{\partial u_z}{\partial z} - \frac{1}{3}\boldsymbol{\nabla}\cdot\boldsymbol{u}\right). \end{aligned}$$

The first term is the usual work by the mean pressure. The second is the extra work due to the pressure anisotropy. In the collisional limit, substitute (4.7) to obtain

$$\boxed{Q_{\rm visc} = \Delta p \left(\frac{\partial u_z}{\partial z} - \frac{1}{3}\boldsymbol{\nabla}\cdot\boldsymbol{u}\right) = 3\eta_\parallel \left(\frac{\partial u_z}{\partial z} - \frac{1}{3}\boldsymbol{\nabla}\cdot\boldsymbol{u}\right)^2 \geq 0.} \tag{4.13}$$

Because $\eta_\parallel > 0$, this contribution always increases the random energy. In the one-dimensional flow of (4.9), it is $Q_{\rm visc} = (4/3)\eta_\parallel(\partial u_z/\partial z)^2$: the same stress that damps the velocity variation heats the plasma.

The energy comes from work done by the flow. Collisions redistribute random energy between directions and make the relaxation irreversible; they do not provide an independent energy source. In fact, the collision terms in (4.1)–(4.2) cancel in the equation for $U = p_\perp + p_\parallel/2$.

The nonnegative square requires the Braginskii closure. In collisionless CGL, Δp retains a dependence on the parcel's history and need not have the same sign as the current difference of stretching rates. The anisotropic pressure work can then have either sign and can reversibly exchange energy with the flow.

General heating formula and the energy equation. For an arbitrary field direction, replace $\partial u_z/\partial z$ by the along-field stretching rate:

$$\boxed{Q_{\rm visc} = \Delta p \left(\boldsymbol{bb} : \boldsymbol{\nabla u} - \frac{1}{3}\boldsymbol{\nabla}\cdot\boldsymbol{u} \right) = 3\eta_\parallel \left(\boldsymbol{bb} : \boldsymbol{\nabla u} - \frac{1}{3}\boldsymbol{\nabla}\cdot\boldsymbol{u} \right)^2 \geq 0.} \tag{4.14}$$

This is sometimes abbreviated as $Q_{\rm visc} = -\boldsymbol{\Pi} : \boldsymbol{\nabla u}$; the colon just sums each stress component times the corresponding velocity gradient, as in the directional calculation above.

Neglecting heat transport and other energy sources, the internal-energy equation is

$$\frac{DU}{Dt} + U\boldsymbol{\nabla}\cdot\boldsymbol{u} = -p\boldsymbol{\nabla}\cdot\boldsymbol{u} + Q_{\rm visc}.$$

Use $U = 3p/2$ and collect the compression terms:

$$\boxed{\frac{Dp}{Dt} + \frac{5}{3}p\boldsymbol{\nabla}\cdot\boldsymbol{u} = \frac{2}{3}Q_{\rm visc}.} \tag{4.15}$$

The left side describes the usual $\gamma = 5/3$ adiabatic pressure response; the right side adds viscous heating. If $Q_{\rm visc} = 0$, continuity gives $D(p/n^{5/3})/Dt = 0$. Positive $Q_{\rm visc}$ raises the pressure above that adiabatic evolution. The same equation follows by taking twice (4.1) plus (4.2), dividing by three, and using (4.11).

We have obtained the *parallel viscosity* part of Braginskii theory. Full collisional transport also includes heat conduction, resistivity, interspecies energy exchange, perpendicular viscosity, and gyroviscosity. Taking $\nu \to 0$ in (4.6) violates its ordering; one must restore pressure evolution instead. An assumed instability-induced scattering rate or a pressure limiter is additional modeling, not a derivation of those Coulomb transport coefficients.

5 Pressure feedback and the parallel firehose

We now turn from collisional relaxation to collective instabilities. Given background pressures $p_\perp$ and $p_\parallel$, we use their stress in the macroscopic force equation to determine whether a bent field line straightens or bends further. This force calculation applies to any gyrotropic background and does not require the Braginskii closure.

5.1 Macroscopic equations and gyrotropic stress

For a quasineutral, fixed-composition plasma whose species share a common bulk velocity, take the leading ideal single-fluid equations

$$\begin{aligned} \frac{D\rho}{Dt} &= -\rho\boldsymbol{\nabla}\cdot\boldsymbol{u}, \\ \rho\frac{D\boldsymbol{u}}{Dt} &= -\boldsymbol{\nabla}\cdot\mathsf{P} + \frac{(\boldsymbol{\nabla}\times\boldsymbol{B})\times\boldsymbol{B}}{4\pi}, \\ \partial_t\boldsymbol{B} &= \boldsymbol{\nabla}\times(\boldsymbol{u}\times\boldsymbol{B}), \qquad \boldsymbol{\nabla}\cdot\boldsymbol{B} = 0. \end{aligned} \tag{5.1}$$

Here $\rho \propto n$. The momentum equation uses pressures summed over species. We neglect Hall, resistive, electron-inertia, and finite-gyroradius corrections. A pressure-dominant ion species with cold electrons gives a simple model for the calculations below; a different electron response must be specified separately.

Together with the pressure evolution laws (3.1), these equations form the double-adiabatic CGL system. The adiabats apply to each species satisfying the assumptions; summed pressures obey them when those species share a flow. For the firehose, we only need the force on a transverse bend.

5.2 Pressure anisotropy changes magnetic tension

Use $\mathsf{P} = p_\perp \mathsf{I} - \Delta p \boldsymbol{bb}$ and $(\boldsymbol{\nabla} \times \boldsymbol{B}) \times \boldsymbol{B} = (\boldsymbol{B} \cdot \boldsymbol{\nabla})\boldsymbol{B} - \boldsymbol{\nabla}(B^2/2)$ to rewrite momentum balance:

$$\boxed{\rho \frac{D\boldsymbol{u}}{Dt} = -\boldsymbol{\nabla}\left(p_\perp + \frac{B^2}{8\pi}\right) + \boldsymbol{\nabla} \cdot \left[\boldsymbol{bb}\left(\frac{B^2}{4\pi} + p_\perp - p_\parallel\right)\right].} \tag{5.2}$$

The coefficient of the bending force is $B^2/(4\pi) + p_\perp - p_\parallel$. Parallel random motions carry momentum along the curved field and oppose its straightening. Thus $p_\parallel > p_\perp$ weakens the magnetic restoring force; a sufficiently large difference reverses its sign.

5.3 Linearize a transverse perturbation

Take a uniform equilibrium $\boldsymbol{B}_0 = B_0 \hat{\boldsymbol{z}}$, with constant $\rho_0, p_{\perp 0}, p_{\parallel 0}$. Let $\delta\boldsymbol{u}_\perp$ and $\delta\boldsymbol{B}_\perp$ vary as $e^{i(k_\parallel z - \omega t)}$. This transverse perturbation has $\delta n = \delta B = 0$ to first order, where δB denotes the change of *field strength*. Induction gives

$$-i\omega\, \delta\boldsymbol{B}_\perp = ik_\parallel B_0\, \delta\boldsymbol{u}_\perp. \tag{5.3}$$

The transverse part of (5.2) is

$$-i\omega\rho_0\, \delta\boldsymbol{u}_\perp = ik_\parallel \left(\frac{B_0^2}{4\pi} + p_{\perp 0} - p_{\parallel 0}\right) \frac{\delta\boldsymbol{B}_\perp}{B_0}. \tag{5.4}$$

The scalar pressure gradient has no transverse component in this geometry. Consequently, the transverse branch does not require a closure for $\delta p_\perp$ or $\delta p_\parallel$. Substitute $\delta\boldsymbol{B}_\perp/B_0 = -k_\parallel \delta\boldsymbol{u}_\perp/\omega$ to obtain

$$\boxed{\omega^2 = k_\parallel^2 \left(v_A^2 + \frac{p_{\perp 0} - p_{\parallel 0}}{\rho_0}\right), \qquad v_A^2 = \frac{B_0^2}{4\pi\rho_0}.} \tag{5.5}$$

For isotropic pressure this is the shear Alfvén wave. With anisotropic pressure it remains an oscillating transverse wave as long as $B_0^2/(4\pi) + p_{\perp 0} - p_{\parallel 0} > 0$. Increasing the parallel pressure reduces this restoring tension. Once the tension becomes negative, $\omega^2 < 0$: the same transverse bend grows exponentially instead of oscillating. The threshold and growth rate are

$$\boxed{p_{\parallel 0} - p_{\perp 0} > \frac{B_0^2}{4\pi}, \qquad \gamma = |k_\parallel| \sqrt{\frac{p_{\parallel 0} - p_{\perp 0}}{\rho_0} - v_A^2}.} \tag{5.6}$$

The long-wavelength parallel firehose is an unstable shear Alfvén mode. Its bending motion has lost its restoring force because the effective magnetic tension has changed sign. This threshold follows from gyrotropic stress, rather than specifically from the compressive CGL closure. The growth rate increases with $|k_\parallel|$ within this approximation; finite-gyroradius physics is needed to determine the fastest-growing scale. Neither this calculation nor the double adiabats determine nonlinear saturation.

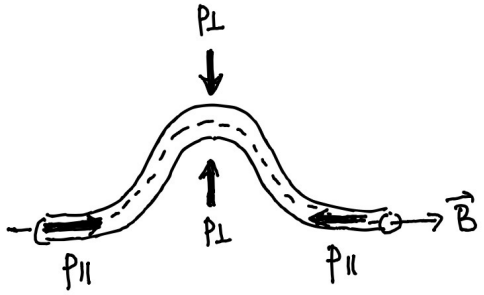


Figure 3: A bent magnetic flux tube in a plasma with $p_\parallel > p_\perp$. Parallel pressure weakens the restoring magnetic tension; when $p_\parallel - p_\perp > B^2/(4\pi)$, the bend grows.

What about $p_\perp > p_\parallel$? The bending force is then stronger, but a compressive instability is possible. That is the mirror problem, where the pressure response can no longer be bypassed.

6 Mirror instability and the Brazil plot

Firehose occurs when the restoring tension of a bending perturbation changes sign. Mirror concerns a different failure: the pressure response that should restore a compression becomes destabilizing. We can explain this feedback without deriving the full kinetic dispersion relation, but its threshold requires the appropriate pressure response.

6.1 Mirror response: a concrete test of the closure

A parcel with $p_\perp > p_\parallel$ has positive tension but can be unstable to a *compressive* disturbance with $k_\perp \gg k_\parallel$. This connects to magnetosheath mirror structures, where magnetic depressions coexist with enhanced particle pressure. For a slow mirror disturbance, perpendicular force balance is approximately

$$\delta\left(p_\perp + \frac{B^2}{8\pi}\right) \simeq 0. \tag{6.1}$$

Whether such a pressure-balanced structure grows depends on how particles redistribute along the field. Magnetic-moment conservation alone does not determine that collective response, and a magnetic depression alone does not identify its generation mechanism.

We state the kinetic threshold here as a comparison, without deriving the kinetic growth rate. For bi-Maxwellian ions, cold electrons, and the long-wavelength, highly oblique marginal limit, kinetic theory predicts

$$\boxed{R - 1 > \frac{1}{\beta_\perp}, \qquad R = \frac{p_\perp}{p_\parallel}, \qquad \beta_\perp = \frac{8\pi p_\perp}{B^2}.} \tag{6.2}$$

This is a kinetic result with specified assumptions. In contrast, the double-adiabatic pressure response gives

$$R > 6\left(1 + \frac{1}{\beta_\perp}\right) \qquad \text{(basic CGL)}. \tag{6.3}$$

Within CGL, the mirror instability is an unstable slow magnetosonic mode: the compressive slow branch changes from $\omega^2 > 0$ to $\omega^2 < 0$. This identifies the CGL branch; it does not make its pressure response or threshold equivalent to the kinetic result. Near kinetic mirror marginality $|\omega| \ll |k_\parallel| v_{\mathrm{th},i}$, where $v_{\mathrm{th},i}$ is the ion thermal speed. Streaming therefore has time to redistribute random energy along the field. Dropping heat-flux effects changes the pressure response and the threshold. Long wavelength and small gyroradius alone do not justify neglecting heat transport.

Mirror: loss of the pressure restoring response. A small magnetic compression, $\delta B > 0$, raises magnetic pressure, which would normally push the plasma back out and oppose the compression. For $p_\perp > p_\parallel$, the static, non-resonant kinetic response instead lowers perpendicular particle pressure in the compressed region. Above the mirror threshold, this decrease outweighs the magnetic-pressure increase: the net static pressure response favors further compression. The reverse perturbation also reinforces itself: a weak-field region develops excess particle pressure and expands further, deepening the magnetic depression (Figure 4).

This reversal identifies the destabilizing feedback. In the kinetic problem, the resonant pressure response from particles with small parallel velocities determines the growth rate and maintains approximate perpendicular pressure balance, (6.1). Near threshold the mirror mode grows without oscillating in the plasma frame. A trapped orbit in Figure 2, by itself, does not establish instability.

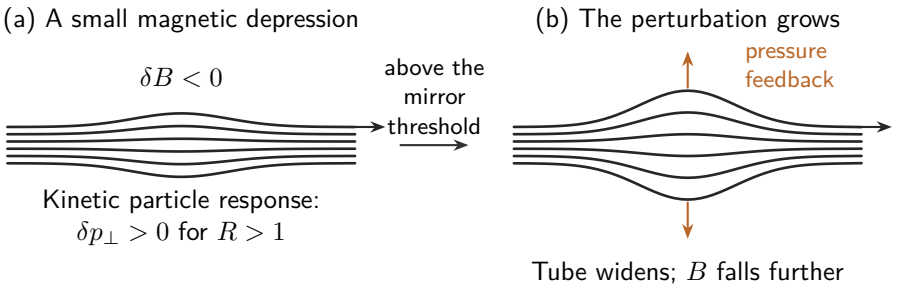


Figure 4: Mirror-instability feedback in the kinetic limit of (6.2). Particle-pressure feedback deepens a magnetic depression, while the resonant response maintains approximate perpendicular pressure balance. Tube-width changes are exaggerated; the sketch illustrates growth, not saturation.

The missing ingredient is the pressure response of particles streaming through the perturbed field. We defer that calculation to the kinetic lecture; the threshold stated here is not a CGL prediction.

6.2 Return to the observations: the Brazil plot

For $p_\perp \simeq p_\parallel \simeq p$, let $\beta = 8\pi p/B^2 \gg 1$. The parallel-firehose and kinetic-mirror boundaries give the approximate interval

$$\boxed{-\frac{2}{\beta} \lesssim \frac{\Delta p}{p} \lesssim \frac{1}{\beta}.} \tag{6.4}$$

Figure 5 places these boundaries in the beta–anisotropy plane. They compare two long-wave limits, not every kinetic instability. The measured distribution and oblique-firehose contours are in Figure 1.

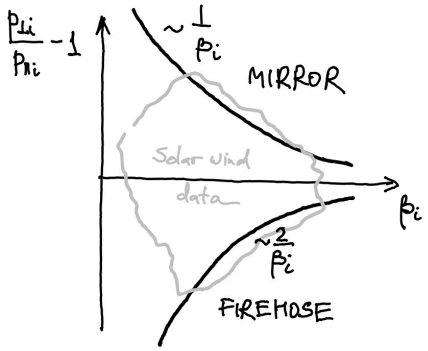


Figure 5: Schematic Brazil plot: $R - 1 = \Delta p/p_\parallel$, with zero at isotropy. The high-beta boundaries are $+1/\beta$ for kinetic mirror and $-2/\beta$ for parallel firehose. The gray outline sketches the occupied solar-wind region; it is not measured data.

Read the plot as drive plus constraint. CGL changes R as $B/n^{2/3}$ changes: radial-field expansion pushes toward the firehose side, while perpendicular compression pushes toward the mirror side. The two instability boundaries approach isotropy as beta increases, explaining why large anisotropies are harder to sustain at high beta. Instability growth and nonlinear feedback can oppose the continuing drive; the observed distribution is not a collection of unrestricted CGL trajectories. The simple parallel-firehose curve illustrates the stress threshold, while the lower envelope of the Wind data is better compared with the oblique kinetic branch.

CGL supplies the drive, linear stability theory locates the onset of growth, and nonlinear dynamics determines the regulation. A threshold alone does not prescribe the rate of scattering or the saturated fluctuation level.

A short modeling connection. One can add an instability-dependent relaxation rate to the pressure equations, or impose a limiter that holds the anisotropy within chosen bounds. A finite relaxation rate allows a response time; a limiter assumes sufficiently rapid regulation at the boundary. These are extra prescriptions. Coulomb relaxation instead acts toward isotropy even within the stable region, and its rapid-collision limit gave Braginskii viscosity in Section 4. Mirror trapping and changes in the field experienced by particles can also regulate anisotropy without being equivalent to pitch-angle scattering.

6.3 Outlook: why we need drift kinetics

A magnetized particle can stream a long distance along the field while remaining close to its guiding-center field line. Small ω/Ω_s and $k\rho_s$ therefore do not ensure negligible heat transport. Near mirror marginality, $|\omega| \ll |k_\parallel| v_{\mathrm{th},s}$: particles have time to redistribute along a perturbation before it changes appreciably.

Drift kinetics evolves the gyrotropic distribution $f(\boldsymbol{x}, v_\parallel, \mu, t)$, retaining parallel streaming, mirror forces, and the parallel electric response. Taking velocity moments gives pressure equations coupled to heat fluxes. Neglecting the heat-flux and collision terms gives double-adiabatic CGL; keeping them requires additional information.

Thus CGL is one fluid limit of a kinetic moment hierarchy. Solving drift kinetics supplies a distribution function and its pressure response; it is not another algebraic option inside an already closed CGL model. In kinetic MHD, those kinetic pressures act in the macroscopic force equation. The mirror problem is our concrete reason to develop that description next.

A kinetic example: electron chorus waves. An anisotropic energetic-electron population can supply energy to whistler-mode chorus through cyclotron resonance; the formation of coherent chorus elements also involves nonlinear wave–particle dynamics. Chorus can then accelerate or scatter energetic electrons, changing radiation-belt electron fluxes.

In the chorus spectrogram, frequency increases vertically and warmer colors indicate stronger wave power. Each strip is a five-second sample, with fifteen minutes between strips.

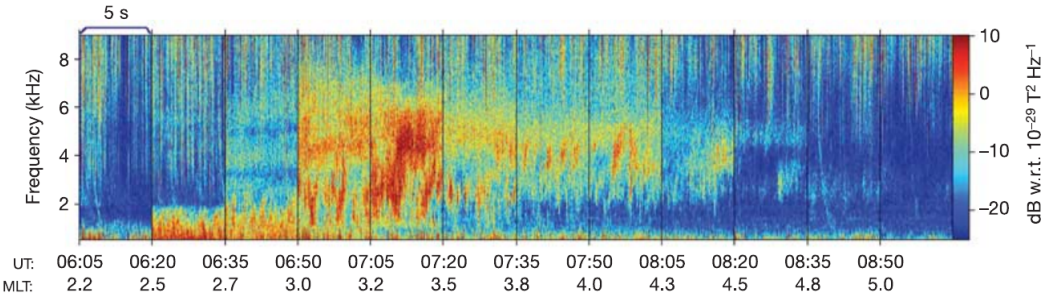


Figure 6: Whistler-mode chorus recorded at Palmer station, Antarctica, on 1 November 2003. The enhanced band lies mainly near 2–6 kHz. UT is universal time and MLT is magnetic local time.

Recommended reading

Main reading. Alexander A. Schekochihin's *Lectures on Kinetic Theory and Magnetohydrodynamics of Plasmas*, especially Sections 24.2.1–24.2.5 (pp. 356–362), covers the pressure equations, double adiabaticity, and the collisional limit. Related material is in Sections 22.7–22.8 (gyrotropic stress and firehose), Section 24.1 (mirror instability), Chapter 23 (drift kinetics), and Chapter 25 (collisional transport).

References

[1] G. F. Chew, M. L. Goldberger, and F. E. Low (1956). The Boltzmann equation and the one-fluid hydromagnetic equations in the absence of particle collisions. *Proceedings of the Royal Society A* **236**, 112–118. doi:10.1098/rspa.1956.0116.

[2] P. Hunana et al. (2019). An introductory guide to fluid models with anisotropic temperatures. Part 1. CGL description and collisionless fluid hierarchy. *Journal of Plasma Physics* **85**, 205850602. doi:10.1017/S0022377819000801.

[3] S. I. Braginskii (1965). Transport Processes in a Plasma. In *Reviews of Plasma Physics*, vol. 1, ed. M. A. Leontovich, pp. 205–311. Original chapter.

[4] T. Berlok, R. Pakmor, and C. Pfrommer (2020). Braginskii viscosity on an unstructured, moving mesh accelerated with super-time-stepping. *Monthly Notices of the Royal Astronomical Society* **491**, 2919–2938. doi:10.1093/mnras/stz3115.

[5] M. W. Kunz, A. A. Schekochihin, and J. M. Stone (2014). Firehose and Mirror Instabilities in a Collisionless Shearing Plasma. *Physical Review Letters* **112**, 205003. arXiv:1402.0010.

[6] P. Hellinger, P. Trávníček, J. C. Kasper, and A. J. Lazarus (2006). Solar wind proton temperature anisotropy: Linear theory and WIND/SWE observations. *Geophysical Research Letters* **33**, L09101. doi:10.1029/2006GL025925.

[7] S. D. Bale, J. C. Kasper, G. G. Howes, E. Quataert, C. Salem, and D. Sundkvist (2009). Magnetic Fluctuation Power Near Proton Temperature Anisotropy Instability Thresholds in the Solar Wind. *Physical Review Letters* **103**, 211101. doi:10.1103/PhysRevLett.103.211101.

[8] R. B. Horne et al. (2005). Wave acceleration of electrons in the Van Allen radiation belts. *Nature* **437**, 227–230. doi:10.1038/nature03939.

[9] Y. Omura, Y. Katoh, and D. Summers (2008). Theory and simulation of the generation of whistler-mode chorus. *Journal of Geophysical Research* **113**, A04223. doi:10.1029/2007JA012622.

[10] D. A. St-Onge, M. W. Kunz, J. Squire, and A. A. Schekochihin (2020). Fluctuation dynamo in a weakly collisional plasma. *Journal of Plasma Physics* **86**, 905860503. arXiv:2003.09760.